



HAL
open science

New Insights Into Processes Controlling the $\delta^{30}\text{Si}$ of Sinking Diatoms: A Seasonally Resolved Box Model Approach

Ivia Closset, Damien Cardinal, Thomas W. Trull, François Fripiat

► **To cite this version:**

Ivia Closset, Damien Cardinal, Thomas W. Trull, François Fripiat. New Insights Into Processes Controlling the $\delta^{30}\text{Si}$ of Sinking Diatoms: A Seasonally Resolved Box Model Approach. *Global Biogeochemical Cycles*, 2019, 33 (8), pp.957-970. 10.1029/2018GB006115 . hal-02402013

HAL Id: hal-02402013

<https://hal.science/hal-02402013>

Submitted on 1 Nov 2021

HAL is a multi-disciplinary open access archive for the deposit and dissemination of scientific research documents, whether they are published or not. The documents may come from teaching and research institutions in France or abroad, or from public or private research centers.

L'archive ouverte pluridisciplinaire **HAL**, est destinée au dépôt et à la diffusion de documents scientifiques de niveau recherche, publiés ou non, émanant des établissements d'enseignement et de recherche français ou étrangers, des laboratoires publics ou privés.

Copyright

Global Biogeochemical Cycles

RESEARCH ARTICLE

10.1029/2018GB006115

This article is a companion to Closset et al. (2015), <https://doi.org/10.1002/2015GB005180>.

Key Points:

- Box model describes properly seasonal variations of surface and water column processes affecting the isotopic composition of biogenic silica
- Maximal rate of silicon uptake in the mixed layer is the most important process controlling the isotopic signatures of biogenic silica
- The Si isotope composition of settling particles records the silicic acid drawdown during the peak of the diatom bloom and not at the end of summer

Supporting Information:

- Supporting Information S1

Correspondence to:

I. Closset,
ivia@ucsb.edu

Citation:

Closset, I., Cardinal, D., Trull, T. W., & Fripiat, F. (2019). New insights into processes controlling the $\delta^{30}\text{Si}$ of sinking diatoms: A seasonally resolved box model approach. *Global Biogeochemical Cycles*, 33, 957–970, <https://doi.org/10.1029/2018GB006115>

Received 18 OCT 2018





Accepted 8 JUL 2019

Accepted article online 17 JUL 2019

Published online 5 AUG 2019

©2019. American Geophysical Union.
All Rights Reserved.

New Insights Into Processes Controlling the $\delta^{30}\text{Si}$ of Sinking Diatoms: A Seasonally Resolved Box Model Approach

Ivia Closset¹ , Damien Cardinal² , Thomas W. Trull^{3,4} , and François Fripiat⁵ 

¹MSI, University of California Santa Barbara, Santa Barbara, CA, USA, ²LOCEAN UMR 7159 Sorbonne Université/CNRS/IRD/MNHN, Paris, France, ³Antarctic Climate and Ecosystems Cooperative Research Center, University of Tasmania, Hobart, Tasmania, Australia, ⁴CSIRO Oceans and Atmosphere, Hobart, Tasmania, Australia, ⁵Max Planck Institute for Chemistry, Mainz, Germany

Abstract In the Southern Ocean, the silicon (Si) biogeochemical cycle is dominated by processes such as the supply of Si into the surface waters, Si uptake into diatom frustules, and their subsequent dissolution and export. Due to the incomplete assimilation of the silicic acid pool (DSi) and isotopic fractionation during silicification, the Si isotopic composition ($\delta^{30}\text{Si}$) of biogenic silica (BSi) is closely linked to the degree of Si utilization in the mixed layer (ML). In this study, we combined modelling approaches and seasonal sediment trap records of $\delta^{30}\text{Si}$ of exported BSi to investigate the magnitude, timing, and isotopic composition of the flux of siliceous particles transferred from the surface to the deep ocean. We implemented a box model to describe the temporal evolution of DSi and BSi concentrations and $\delta^{30}\text{Si}$ in the ML and at depth. The model allows us to quantify fluxes of Si in and out of the ML associated with export, dissolution, and mixing. It highlights that the time-integrated $\delta^{30}\text{Si}$ of exported BSi measured in the sediments reflects the extent of DSi consumption at the time when net BSi production and diatom accumulation are maximal in the ML and confirms that the $\delta^{30}\text{Si}$ of diatoms is a reliable proxy for past Si utilization.

1. Introduction

Diatoms, a siliceous group of phytoplankton, constitute the main vector of the biological carbon pump south of the Subantarctic Front and create a strong connection between the biogeochemical cycling of silicon (Si) and carbon (C). In the Southern Ocean, Si is mainly supplied to the surface waters through vertical mixing via the meridional overturning circulation and winter convection. In the euphotic zone, diatoms consume silicic acid (or dissolved Si, hereafter referred to as DSi) to build their cell wall or frustule (hereafter referred to as biogenic silica, BSi). Approximately 30% to 60% of their production is directly recycled in the surface ocean (Holzer et al., 2014; Tréguer & De la Rocha, 2013) while the rest is exported below the mixed layer (ML) along with some organic carbon. BSi partially dissolves in its downward flux through the deep ocean and particles that are not recycled are finally buried into the sediment. Since the residence time of Si in the ocean is relatively long (between 15,000 and 17,000 years; Tréguer & De la Rocha, 2013), variations in DSi concentrations observed in the ocean are mainly linked to both the activity of diatoms in surface waters as well as dissolution at depth. Coupled to northward Ekman transport, this biological activity generates a strong gradient of DSi across the Antarctic Circumpolar Current (ACC; Ragueneau et al., 2000; Sarmiento et al., 2004). South of the Polar front (PF), surface waters support seasonal blooms of diatoms, which promote high BSi export to the ocean interior, and ultimately high BSi accumulation rates in sediments (DeMaster, 1981) with an overall estimate for the Southern Ocean burial rate of $2.0 \pm 1.2 \text{ Tmol Si year}^{-1}$ (Tréguer, 2014). The BSi that is not buried into the sediments is recycled in the water column and trapped in the Antarctic bottom waters (Holzer et al., 2014) and/or exported toward lower latitudes via the subduction and northward advection of Antarctic Intermediate waters and Subantarctic mode waters. The Southern Ocean is thus the most important sink of silica in the world ocean (Pondaven et al., 2000) and a key region for the control of low-latitude nutrient supply and biological productivity (Sarmiento et al., 2004). Therefore, examining the modern biogeochemical cycle of Si in the Southern Ocean and quantifying the different stocks and fluxes are of major interest in marine and climatic sciences. However, estimation of the Si mass balance in the ocean from direct measurements is difficult due to the strong spatiotemporal variability (notably the seasonal cycle in the euphotic zone) of the surface ocean.

The isotopic composition of Si ($\delta^{30}\text{Si}$) is a valuable proxy to assess temporal and spatial variabilities of the Si cycle in both modern and past oceans since it can potentially resolve the processes involved in marine biogeochemical cycling of Si. In the ocean, the stable Si isotope composition of both DSi and BSi pools is expressed in ‰ as follows:

$$\delta^{30}\text{Si} = \left(\frac{{}^{30}\text{R}_{\text{sample}}}{{}^{30}\text{R}_{\text{standard}}} - 1 \right) * 1000 \quad (1)$$

where ${}^{30}\text{R}_{\text{sample}}$ and ${}^{30}\text{R}_{\text{standard}}$ are the atomic ratios of heavy (${}^{30}\text{Si}$) and light (${}^{28}\text{Si}$) isotopes of Si (${}^{30}\text{Si}/{}^{28}\text{Si}$) of the sample and international reference NBS28 quartz standard, respectively. During silicification, diatoms fractionate Si isotopes and preferentially take up ${}^{28}\text{Si}$ (De la Rocha et al., 1997) leaving the residual DSi pool relatively enriched in ${}^{30}\text{Si}$. This leads to a general inverse relationship between DSi concentration and $\delta^{30}\text{Si}$ due to the progressive increase in $\delta^{30}\text{Si}$ of both substrate ($\delta^{30}\text{Si}_{\text{DSi}}$) and product ($\delta^{30}\text{Si}_{\text{BSi}}$) as the nutrient pool is consumed (e.g., Cavagna et al., 2011; Varela, Pride, & Brzezinski, 2004). This preferential uptake is characterized by a fractionation factor (${}^{30}\epsilon$) averaging $-1.2\text{‰} \pm 0.2\text{‰}$ in the Southern Ocean (Fripiat et al., 2011b). Recent studies have shown that seasonal, species or regional variations in ${}^{30}\epsilon$ can occur (e.g., Fripiat et al., 2012; Sutton et al., 2013) and that contrary to what has been considered so far, the fractionation factor might be more variable than expected.

The isotopic imprint of diatom production can be measured directly in seawater and/or particles in the water column and recorded in the BSi preserved in the sediments. In a paleoceanographic perspective, $\delta^{30}\text{Si}$ signatures have been used to trace nutrient utilization in past oceans and to study the role of Southern Ocean productivity in the fluctuations of atmospheric CO_2 over glacial cycles or during the Holocene (e.g., Brzezinski et al., 2002; De La Rocha et al., 1998; Panizzo et al., 2014). Two relatively simple models are generally used to estimate the Si utilization in palaeoceanographic studies. (i) In the closed system (also referred to as Rayleigh model), the surface ocean has a limited pool of DSi, supplied at the beginning of the growth period (e.g., by winter convection), that is progressively consumed by diatoms and exported to the deep ocean. The reaction progresses consuming substrate (here silicic acid) and increasing exponentially its $\delta^{30}\text{Si}$ (equation (2); Fry, 2006). There are two products in the closed system, the instantaneous BSi product that exhibits a constant offset from the dissolved Si substrate at any time (equation (3)) and the accumulated product (equation (4)) that eventually exhibits the same $\delta^{30}\text{Si}$ as the initial substrate (equation (2)) when the reaction is complete:

$$\delta^{30}\text{Si}_{\text{sub}} = \delta^{30}\text{Si}_{\text{init}} - {}^{30}\epsilon \ln(1-f) \quad (2)$$

$$\delta^{30}\text{Si}_{\text{inst}} = \delta^{30}\text{Si}_{\text{sub}} + {}^{30}\epsilon \quad (3)$$

$$\delta^{30}\text{Si}_{\text{acc}} = \delta^{30}\text{Si}_{\text{init}} + {}^{30}\epsilon \left(\frac{f \times \ln f}{1-f} \right) \quad (4)$$

In these equations, ${}^{30}\epsilon$ is the isotope effect (in ‰) of the reaction, f is the fraction of the remaining substrate, and the subscripts “sub,” “init,” “acc,” and “inst” refer to the remaining substrate, the initial substrate, the accumulated product and the instantaneous product, respectively. (ii) In the open system (also referred to as steady-state model), a continuous supply of substrate balances the export of product and residual substrate. The isotopic compositions of DSi and BSi display linear changes and there is no accumulated product in that case (equations (5) and (6); Fry, 2006):

$$\delta^{30}\text{Si}_{\text{sub}} = \delta^{30}\text{Si}_{\text{init}} - {}^{30}\epsilon(1-f) \quad (5)$$

$$\text{Si}_{\text{inst}} = \delta^{30}\text{Si}_{\text{init}} + {}^{30}\epsilon \times f \quad (6)$$

While the closed and open models have been used successfully for interpreting paleoceanographic isotopes records, the distinction between these two simple models in the modern ocean can be difficult. Some regions have been shown to switch between closed and open system dynamics (e.g., in the Kerguelen Plateau area; Closset et al., 2016) depending on their DSi uptake: DSi-supply ratio or on their BSi accumulation: BSi export ratio. The $\delta^{30}\text{Si}_{\text{BSi}}$ and $\delta^{30}\text{Si}_{\text{DSi}}$ can also be affected differently, since the BSi pool is composed of a mix of newly formed (and isotopically light) diatoms as well as isotopically heavy diatoms that were produced earlier in the ML (see Closset et al., 2015). It is therefore not obvious how to best describe the silicon mass and

isotopic variations in the modern Southern Ocean or how to reconstruct past processes from exported particle signatures. More explicitly, none of these models have the time parameter in their equations; they thus are inherently unsuited to track seasonal variations. We need to design a model that describes more fully the processes involved in seasonal variations of $\delta^{30}\text{Si}$ to improve estimates silicon cycling in the ocean.

Moreover, exchanges between dissolved and particulate phases (e.g., dissolution of BSi) as well as physical transport or mixing of DSi may also modify the apparent $^{30}\epsilon$ and alter the evolution of $\delta^{30}\text{Si}$ of BSi and DSi from the theoretical trends predicted by these models. The global ocean (including the Southern Ocean) is undersaturated with opal; hence, the BSi constituting diatom frustule is subjected to dissolution if not protected by the cell membrane. The processes of BSi production and dissolution are decoupled in time since it is only after cell death and the degradation of the protecting organic matter layer surrounding the frustule that BSi begins to dissolve (Bidle & Azam, 1999). Demarest et al. (2009) have reported that the light ^{28}Si preferably dissolves with a fractionation factor of -0.55‰ . However, this isotopic fractionation linked to BSi dissolution is debated due to the observations of homogeneous $\delta^{30}\text{Si}$ depth profiles of suspended BSi (e.g., Fripiat et al., 2012), the similarity of $\delta^{30}\text{Si}$ of core top and surface water BSi (e.g., Egan et al., 2012), as well as a recent evidence for a lack of isotopic fractionation during dissolution of sedimentary diatoms in laboratory experiments (Wetzel et al., 2014). Addressing these uncertainties has important implications in paleoceanography, because historical estimates of paleovariations in diatom DSi consumption have used either the Rayleigh model or the steady-state model, ignoring potential biases linked to water mass mixing as well as water column and sedimentary BSi dissolution.

To date, only three papers have attempted to describe the seasonal Si biogeochemical and isotopic cycle in the Southern Ocean using modelling approaches (Coffineau et al., 2014; De Brauwere et al., 2012; Fripiat et al., 2012). None of them consider the history of particles during their descent through the water column nor do they integrate the seasonality of parameters that control the recycling of BSi at depth. They therefore poorly describe the export and recycling of BSi and how these processes affect the isotopic signature of exported BSi, which is the parameter we measure and interpret in paleoceanography.

Here we investigate the Si biogeochemical cycle from the surface to the deep ocean using a combination of modelling and previously published seasonal records of exported BSi $\delta^{30}\text{Si}$ (Closset et al., 2015). Closset et al. (2015) examined the Subantarctic Zone (SAZ), polar front zone (PFZ), and Antarctic zone (AZ). The SAZ is a more active region in terms of mixing than the ACC south of the SAF and isotopic reactions are unlikely to follow the same dynamics as in the AZ. Furthermore, diatoms do not dominate the primary and export production in the SAZ. For these reasons, this study focuses on processes occurring south of the Subantarctic Front. The model presented here differs from previous models as it integrates processes that affect the fate of particles in the deep ocean which affect the magnitude of BSi recycling throughout the water column. Our specific objectives are as follows.

1. Reconstruct the seasonal and spatial variations of the exported BSi $\delta^{30}\text{Si}$.
2. Use exported $\delta^{30}\text{Si}$ signatures to identify and quantify processes impacting the BSi production and Si cycle in the ML.
3. Determine whether the Si-pool in the ML operates in an open or closed system and refine the fractionation factor in the Southern Ocean.
4. Investigate the effect of fractionation during BSi dissolution on the isotopic signature of particles that reach the sediment.

2. Material and Methods

2.1. Sample Collection, Processing, and Isotopic Measurements

Sinking particles were collected from four sediment traps (McLane Inc., Parflux 21 sampling cups) that were deployed at two open ocean moorings in the Antarctic Zone (61°S , AZ, 2,000 and 3,700 m) and the Polar Front Zone (54°S , PFZ, 800 and 1,500 m) along 140°E in the Australian Sector. Sampling intervals were programmed to be short (8–10 days) in summer and longer (up to 60 days) in winter, allowing high sampling resolution during the austral summer. A description of the physical environment and detailed methods for sediment trap sample processing are reported in Closset et al. (2015). Briefly, after BSi extraction, samples were purified and analyzed for Si isotopic composition on a Neptune + MC-ICP-MS, using Mg external

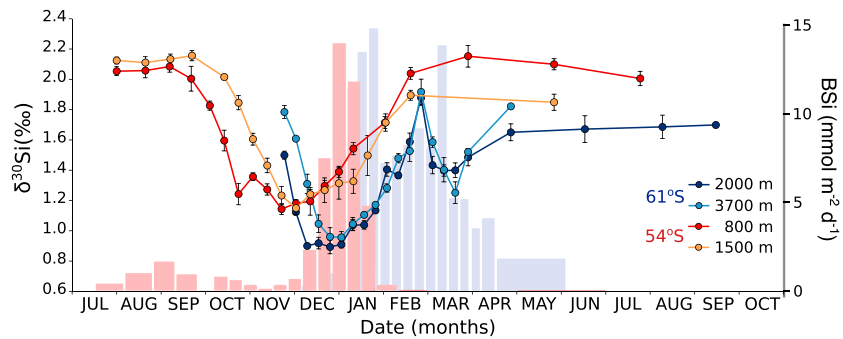


Figure 1. Seasonal variations of silicon isotopic composition ($\delta^{30}\text{Si}$) of settling particles collected by sediment traps in the Antarctic (61°S) and the Polar Front (54°S) Zone, along with BSi flux collected into the traps (in $\text{mmol m}^{-2} \text{d}^{-1}$) in the AZ (blue bars) and in the PFZ (red bars). Data from Closset et al., 2015.

doping in dry plasma mode. The average reproducibility of the full chemical procedure was $\pm 0.05\text{‰}$ (± 1 sd). Measurement accuracy was controlled using a secondary reference material (diatomite, $\delta^{30}\text{Si} = 1.28\text{‰} \pm 0.05\text{‰}$, 1 sd) whose Si-isotopic composition has been previously characterized ($1.26\text{‰} \pm 0.2\text{‰}$; Reynolds et al., 2007).

Closset et al. (2015) have described and discussed the seasonal variations of BSi flux and $\delta^{30}\text{Si}$ of settling particles collected south of the SAF from this sediment trap time series (Figure 1). They reported that the lowest $\delta^{30}\text{Si}$ occurred at the onset of diatom export and could be considered as spring values for diatoms blooming in the ML. $\delta^{30}\text{Si}$ signatures became gradually heavier as the flux of BSi collected in the traps became maximum recording production and particle export from surface waters. Thereafter, it remained heavy and constant during winter when BSi flux was low. The authors suggested that diatoms displaying a $\delta^{30}\text{Si}$ typical of late summer conditions continue to collect slowly in deep traps several months after the end of the growing season, generating a weak flux of isotopically heavy particles. In early spring, the $\delta^{30}\text{Si}$ signal began to decrease progressively following initiation of export production from surface waters and increased of BSi flux in the trap. This progressive lightening likely implies that the flux of particles is composed by a mix of old and isotopically heavy diatom fragments with more recent and isotopically light particles formed during the spring bloom.

2.2. Determination of the Fractionation Factor and Initial Conditions

The fractionation factor of DSi uptake by Antarctic diatoms was previously estimated to be $-1.2\text{‰} \pm 0.2\text{‰}$ (Fripiat et al., 2011b). However, this value reflects a mean estimate from several different cruises and might not suit our specific environment. Here we reevaluate both the mean and variability of $^{30}\epsilon$ using the exported biogenic silica $\delta^{30}\text{Si}$ from our sediment trap time-series.

Since ML isotopic composition and DSi concentrations were measured at 61°S shortly after the date when moorings were deployed ($1.90\text{‰} \pm 0.08\text{‰}$ and $28.1\text{ }\mu\text{mol/L}$, respectively; Cardinal et al., 2005) and at 54°S two years after those moorings were installed (1.99‰ and $11\text{ }\mu\text{mol/L}$, respectively; Cardinal et al., 2005), and since these samples have been collected in early spring, we can assume that they are appropriate initial values to simulate the evolution of $\delta^{30}\text{Si}$ following a closed model (Figures 2a and 2c) or a steady-state model (Figures 2b and 2d). The initial DSi inventory integrated over the ML (97 m in the AZ and 76 m in the PFZ; Cardinal et al., 2005) was therefore 1.36 and 0.42 moles in the AZ and PFZ, respectively.

In the ACC, Holzer et al. (2014) estimated that 50% of the BSi exported from the ML is dissolved above 2,000 m. By first correcting our BSi fluxes for such dissolution effects, we can estimate the seasonal DSi consumption in the ML at 61°S and 54°S (equal to the integrated corrected BSi collected in the traps) and thus the fraction of DSi-stock remaining in the ML (notated f in equations (2) to (6)). To limit possible bias on $^{30}\epsilon$ estimates due to Si-source choice and to optimize the $^{30}\epsilon$ for our exported BSi data set, we have extracted this parameter using an iterative optimization algorithm (Levenberg Marquardt) that minimizes the quantity $\chi^2 = \sum_i |r_i|^2$, where r_i are the residuals giving the difference between each original data point and its fitted value (see Table S1 in the supporting information). Applying this method on the $\delta^{30}\text{Si}$ of exported BSi

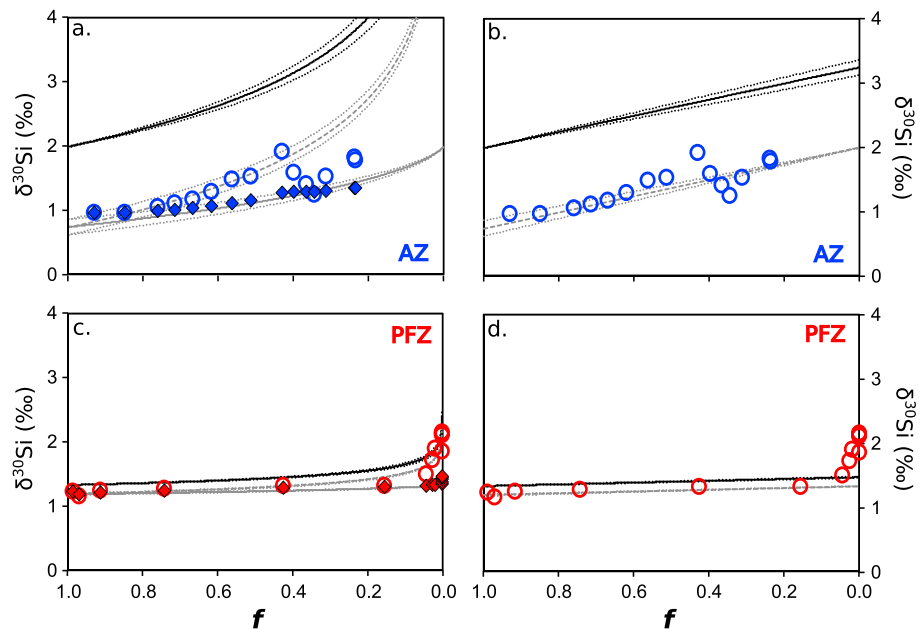


Figure 2. $\delta^{30}\text{Si}$ variations of settling BSi in the AZ (2,000 m, blue dots) and the PFZ (800 m, red dots) described following a Rayleigh distillation model (a and c) or a steady state fractionation model (b and d). The black line represents the evolution of $\delta^{30}\text{Si}$ of the remaining dissolved pool in the mixed layer, gray lines are the evolution of $\delta^{30}\text{Si}$ of exported BSi, with plain and dashed line associated to accumulated and instantaneous product, respectively, in the case of a Rayleigh distillation model. Dotted lines indicate ± 1 sd of the fractionation factor and f is the fraction of DSi remaining in the pool. Diamonds represent the evolution of time integrated $\delta^{30}\text{Si}$ (see text for details). AZ = Antarctic Zone; PFZ = Polar Front Zone.

measured during the productive period in the traps and considering that the system follows a Rayleigh fractionation law from the beginning of production to the mixing event(s) (i.e., in March) in the AZ and to the end of the bloom (i.e., in June) in the PFZ, we can estimate a $^{30}\epsilon$ associated with our sediment trap data set ranging from $-0.98\text{‰} \pm 0.13\text{‰}$ in the AZ to $-1.13\text{‰} \pm 0.16\text{‰}$ in the PFZ. These estimates are particularly coherent with previous estimates from the same transect in the ML and subsurface (Cardinal et al., 2005), as well as the fractionation factor estimated for the Southern Ocean (Fripiat et al., 2011b), suggesting limited variation of $^{30}\epsilon$. Moreover, using the iterative optimization algorithm, we are able to refine the initial $\delta^{30}\text{Si}$ in the AZ ($1.71\text{‰} \pm 0.08\text{‰}$) and in the PFZ ($2.1\text{‰} \pm 0.1\text{‰}$), values which are not significantly different from those measured in 2001 by Cardinal et al. (2005), 1.90‰ and 1.99‰ , respectively.

2.3. Model Parametrization

To better assess the processes controlling the seasonal evolution of exported BSi $\delta^{30}\text{Si}$ south of the SAF, we have implemented a box-model based on conservation of Si mass and isotopic composition. In addition to previous models, this one considers the seasonal variability of parameters that affect the Si biogeochemical cycle and that were not taking into account in previous models (such as changes in irradiance, MLD, or sinking velocities of particles). The model was adjusted using parameters estimated from the sediment trap time series, observed ML climatology (given in Closset et al., 2015) and data measured by Cardinal et al. (2005). The aim was to create a simple yet reasonably realistic model to assess the influence of different biogeochemical and physical processes on the seasonal evolution of isotopic composition of exported and potentially buried BSi.

Figure 3 describes the model structure which consisted of one box representing the surface ML, with deep waters as boundary conditions. The ML contains two compartments corresponding to the DSi and BSi pools while the deep-water box displays only the BSi pool. The Si concentrations and isotope compositions in the different compartments vary with time due to uptake, dissolution, export, and mixing that transfer mass and/or isotopes between the pools (arrows in Figure 3). The concentration and $\delta^{30}\text{Si}$ in the Winter Water (WW) DSi pool remain constant in the box model. The WW is the remnant of the previous winter mixed

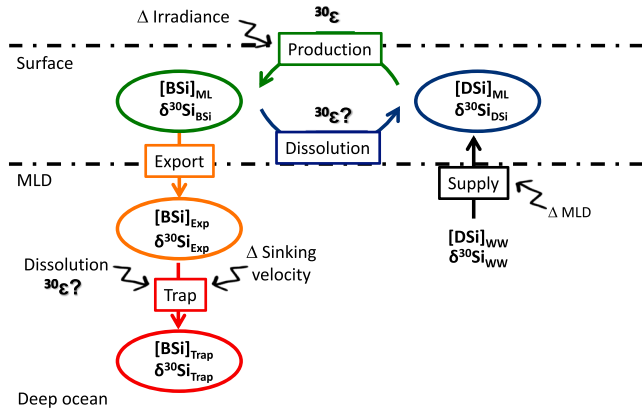


Figure 3. Schematic representation of the box model. Round boxes represent pools of DSi and BSi in the ML (blue and green, respectively), the shallow export of BSi (orange), and the deep export of BSi (red). Arrows stand for processes exchanging Si between the pools: vertical DSi supply (black), gross BSi production (green), BSi dissolution (blue), BSi export below the ML (orange), and BSi export at depth (red). Small black arrows represent the additional parameters that constrain the fluxes of Si between the boxes: seasonal variation of MLD (from ARGO data set; Closset et al., 2015), irradiance and particles sinking velocities (from Closset et al., 2015), and dissolution at depth. ML = mixed layer.

layer and is usually identified by the minimum of temperature centered around 200 m. It has the same DSi concentration as surface layer in winter (before any diatom uptake) and is the proximal source of the DSi supply to the surface, owing to its position between the ML and deep waters. To keep the model simple, we assume that the deep BSi dissolution does not significantly control the concentration of DSi in the deep ocean, which seems to be a reasonable assumption. Indeed, in the ocean, the deep DSi stock is linked to a combination of cumulated BSi dissolution along the thermohaline circulation and preformed nutrients (De Souza et al., 2014), with little contribution from in situ BSi dissolution, and for deepest sample, from benthic diagenesis (Tréguer & De La Rocha, 2013). Considering that the DSi and BSi pools in the ML are homogeneous, the seasonal evolution of each compartment in the model can be described as follows:

$$\frac{dDSi_{ML}}{dt} = DSi_{supply} + D_{ML} - GrossP \quad (7)$$

$$\frac{dBSi_{ML}}{dt} = GrossP - D_{ML} - E_{ML} \quad (8)$$

$$\frac{dBSi_{exp}}{dt} = E_{ML} - E_{deep} \quad (9)$$

$$\frac{dBSi_{trap}}{dt} = E_{deep} - D_{deep} \quad (10)$$

where DSi_{ML} and BSi_{ML} are the DSi and BSi concentration in the ML, BSi_{exp} is the BSi concentration exported just below the ML and BSi_{trap} is the BSi concentration collected in the trap. DSi_{supply} is the upward supply of DSi to the ML; D_{ML} and D_{deep} are the dissolution in the ML and at depth; $GrossP$ is the gross production of biogenic silica in the ML; E_{ML} and E_{deep} are the export fluxes of diatom out of the ML (i.e., the BSi flux calculated just below the ML) and at depth (i.e., the BSi flux collected in the sediment trap), respectively. (See section 2.4 for further description of these parameters.)

In the model, the ratios (R) of silicon isotopes ($^{30}\text{Si}/^{28}\text{Si}$) for all the compartments were calculated by considering isotopic fractionation during DSi uptake and/or BSi dissolution (in the ML and at depth). Since the occurrence of Si isotopic fractionation during BSi dissolution remains uncertain, the model was run with and without fractionation during dissolution to compare the predicted $\delta^{30}\text{Si}$ of exported BSi with our sediment trap time series. No fractionation was ascribed for the DSi supply to the ML nor for the BSi settling process as they are considered in the model as purely mechanical processes.

$$\frac{dRDSi_{ML}}{dt} = DSi_{supply} \times RDSi_{supply} + D_{ML} \times (\alpha_{diss} \times RBSi_{ML}) - GrossP \times (\alpha_{prod} \times RDSi_{ML}) \quad (11)$$

$$\frac{dRBSi_{ML}}{dt} = GrossP \times (\alpha_{prod} \times RDSi_{ML}) - D_{ML} \times (\alpha_{diss} \times RBSi_{ML}) - E_{ML} \times RBSi_{ML} \quad (12)$$

$$\frac{dRBSi_{exp}}{dt} = E_{ML} \times RBSi_{ML} - E_{deep} \times RBSi_{exp} \quad (13)$$

$$\frac{dRBSi_{trap}}{dt} = E_{deep} \times RBSi_{exp} - D_{deep} \times (\alpha_{diss} \times RBSi_{exp}) \quad (14)$$

In these equations, α_{prod} and α_{diss} are the isotopic fractionation factors for BSi production and dissolution, respectively ($\alpha = \delta^{30}\text{Si}/1,000 + 1$; see Table 1). $\delta^{30}\text{Si}$ values were then back calculated using equation (1).

2.4. Boundary Conditions

For each simulation, the model was run for one year starting at the beginning of summer in each zone (November in the AZ and September in the PFZ). In the Southern Ocean, phytoplankton activity is

Table 1
Box-model processes and parameters applied for the PFZ and the AZ

| Processes | Parameters | Unit | PFZ | AZ |
|-------------|-------------------|-------------------|-------------------|-------------------|
| | | | mean ± <i>sd</i> | mean ± <i>sd</i> |
| Uptake | V_{max} | d^{-1} | 0.34 ± 0.02 | 0.30 ± 0.02 |
| | k_{Si} | $\mu\text{mol/L}$ | 4.00 ± 0.20 | 3.50 ± 0.18 |
| Dissolution | ϵ_{prod} | $\%$ | -1.13 ± 0.16 | -0.98 ± 0.13 |
| | V_{dissML} | d^{-1} | 0.035 ± 0.002 | 0.035 ± 0.002 |
| | $V_{dissDeep}$ | d^{-1} | 0.016 ± 0.001 | 0.090 ± 0.005 |
| Export | ϵ_{diss} | $\%$ | -0.55 ± 0.05 | -0.55 ± 0.05 |
| | V_{Exp} | d^{-1} | 0.13 ± 0.01 | 0.13 ± 0.01 |

Note. Parameters were estimated from this study, Kamatani (1982), Ragueneau et al. (2000), Franck et al. (2003), Demarest et al. (2009), and Closset et al. (2014). AZ = Antarctic Zone; PFZ = Polar Front Zone.

mainly constrained by macronutrient and micronutrient availability (e.g., DSi and/or Fe) as well as light limitation. The light regime is highly seasonal south of the SAF, characterized by a long period of low solar irradiance (winter) that prevents diatom growth, followed by a short period (summer) of favorable light conditions for photosynthesis. The light limitation of diatom growth is simulated by a dimensionless parameter varying between 0 (in winter) and 1 (in summer) that modulates the intensity of the diatom uptake:

$$LightLimitation = 1 - e^{-\frac{0.1xI}{pMax}} \quad (15)$$

where $pMax$ is the maximal photosynthetic rate (d^{-1}) given in Eppley (1972) and I is the mean photosynthetically active radiation (PAR; W/m^2) in the ML. To simplify the model and because our light parameter

is only used as a limitation function, I was approximated using a sinusoidal function ($\sin((\text{time}/10) \times 0.24) \times 50$, with time—in days—starting the first day of the model simulation) that ranges between 0 and 50, simulating expected daily PAR in the ML. Note that we set $PAR = 0$ when this sinusoidal function gives negative values of PAR. This allows the productive period to have a duration of 90 days with a peak occurring in November–December, consistent with the satellite-based observations of these two regions (see Rigual-Hernández et al., 2015; 2016).

The vertical supply of DSi to the ML originates from ML deepening and subsequent DSi detrainment into surface waters. To simplify the equations, DSi supply via vertical diffusion was ignored. In the model, Mixed layer depths (MLD) were extracted from the Argo data set (www.argo.ucsd.edu) and were calculated from individual Argo profiles using a surface-density-difference criterion of 0.03 kg/m^3 (see Closset et al., 2015; Sallée et al., 2006). This provided monthly MLD estimates on a half-degree grid, which were then used to obtain daily estimates of DSi supply to the ML as follows:

$$DSi_{supply} = DSi_{WW} \times \frac{\left(\frac{dZ}{dt}\right)}{Z} \quad (16)$$

where DSi_{WW} ($\mu\text{mol/L}$) is the silicic acid concentration in the Winter Water pool and Z is the depth of the ML (m). Note that we did not consider any deentrainment of DSi or BSi from the ML to the WW when MLDs shoaled (i.e., when dZ is <0 , DSi supply = 0).

The uptake of DSi during the productive period is well described using a Michaelis-Menten saturation function (Paasche, 1973) modulated by seasonal light variations:

$$V_{Si} = \frac{V_{max} \times DSi_{ML}}{k_{Si} + DSi_{ML}} \times LightLimitation \quad (17)$$

where V_{Si} is the specific DSi uptake rate (d^{-1}), V_{max} (d^{-1}) is the maximum or saturated uptake rate, k_{Si} ($\mu\text{mol/L}$) is the half saturation constant of DSi uptake, and DSi_{ML} ($\mu\text{mol/L}$) is the silicic acid concentration in the ML. In this equation, the diatom uptake rate is governed by the availability of DSi (substrate) and by the light limitation term calculated previously (equation (15)). The gross BSi production (in $\mu\text{mol L}^{-1} d^{-1}$) was then calculated from

$$GrossP = V_{Si} \times BSi_{ML} \quad (18)$$

where BSi_{ML} ($\mu\text{mol/L}$) is the biogenic silica concentration in the ML.

In the box model, we distinguished two dissolution fluxes. The dissolution in the ML (D_{ML} , $\mu\text{mol L}^{-1} d^{-1}$; equation (19)) is described by a first order equation proportional to the amount of substrate.

$$D_{ML} = V_{dissML} \times BSi_{ML} \quad (19)$$

where V_{dissML} is the specific remineralization rate of diatoms (d^{-1}).

The amount of BSi dissolved at a given depth z below the mixed layer (D_{deep} , $\mu\text{mol L}^{-1} \text{d}^{-1}$; equation (20)) depends on particle sinking velocities (S_p , m/d), as this determines the time a particle spends within a given depth interval. Thus, the faster the particle sinks, the lower the dissolution flux. This parameter varies on a seasonal timescale, and values used in the model are derived from the $\delta^{30}\text{Si}$ value of the particles flux (Closset et al., 2015).

$$D_{deep} = BSi_{exp} \times e^{\left(-V_{dissDeep} \times \frac{H-z}{S_p}\right)} \quad (20)$$

where BSi_{exp} ($\mu\text{mol/L}$) is the biogenic silica pool exported from the ML, $V_{dissDeep}$ is the specific remineralization rate of particles at depth (d^{-1}), and H (m) is the depth of the sediment trap that collected particles.

Similarly, we have defined two export fluxes. First, the flux of BSi that is exported from the ML (E_{ML} , $\mu\text{mol L}^{-1} \text{d}^{-1}$) was calculated as (using the first order constant V_{exp} , d^{-1}):

$$E_{ML} = V_{exp} \times BSi_{ML} \quad (21)$$

Second, the flux of BSi exported to depth (E_{deep} , $\mu\text{mol L}^{-1} \text{d}^{-1}$) to be collected in the sediment traps was estimated based on particle sinking velocities (S_p) and biogenic silica dissolution at depth (D_{deep}). In other words, the flux of silica leaving the ML is attenuated in proportion to the time spent in deep waters before reaching the traps, and particles are redistributed in the trap depending on their time spent in the water column. Particles that were produced at different times within the ML can simultaneously reach the same sediment trap and be part of the same time interval of deep flux of exported BSi.

Most of the parameter values used in equations (15) to (21) are derived from the literature, that is, they were not selected by matching the model to observations and are given in Table 1.

3. Results and Discussion

3.1. Mass and Isotopic Balance of Exported BSi South of the SAF

Our results show that south of the PF, the $\delta^{30}\text{Si}$ of exported BSi differs markedly from that predicted by steady-state model, especially during the growth season (i.e., at $0.3 < f < 0.6$ which corresponds to January/February; Figures 2b and 2d). Even if the ML did not strictly follow a closed system during the productive period, the dynamics of diatom blooms consuming surface water DSi was better described by a closed system Rayleigh fractionation law (Figures 2a and 2c). Indeed, as already reported by Fripiat et al. (2012) during this period, the ML was highly stratified and nutrient uptake would have greatly exceeded new input from vertical mixing inducing a low Si supply: Si-uptake ratio. The production of BSi progressed in a sequential mode over time, consuming substrate (silicic acid) present at the beginning and exporting instantaneous product (exported BSi sequentially collected in the traps). Moreover, the time-integrated isotopic signature of exported BSi fits well the accumulated product (Figures 2a and 2c) both in the AZ and the PFZ. Occasionally, mixing event(s) disrupted the ML (e.g., in March in the AZ), resulting in an increase of the Si supply: Si-uptake ratio leading to a lighter (lower) $\delta^{30}\text{Si}$ signal for the instantaneous product (exported BSi collected in the traps). This can be thought of as either a resetting of the closed system back toward initial conditions or a shifting of the system toward an open steady-state mode. Thus, while the Rayleigh model reasonably describes the system during the production period and for the seasonally integrated biogenic silica export, it does not accurately elucidate the seasonal variations of exported BSi $\delta^{30}\text{Si}$ in these regions for specific time-periods (i.e., late summer or following mixing events). During these times, evolution of $\delta^{30}\text{Si}$ is affected by additional processes including Si-supply into the ML, dissolution of BSi, and variations in the fractionation factors associated with silicic acid uptake due to changing environmental conditions.

Using the $^{30}\epsilon$ and initial parameters estimated in this study, variations of $\delta^{30}\text{Si}$ and estimate Si fluxes in the ML during the bloom period can be reconstructed. Note that we use first the shallower traps (2,000 m in the AZ and 800 m in the PFZ) which presents the longest $\delta^{30}\text{Si}$ record. When working with the two theoretical models, cups that have collected particles before the beginning of the DSi consumption in the ML were not considered, because those particles likely originate from the previous season (Closset et al., 2015). The Rayleigh fractionation law predicts that 31% of the initial pool of DSi (i.e., the 28.1 $\mu\text{mol/L}$; Cardinal

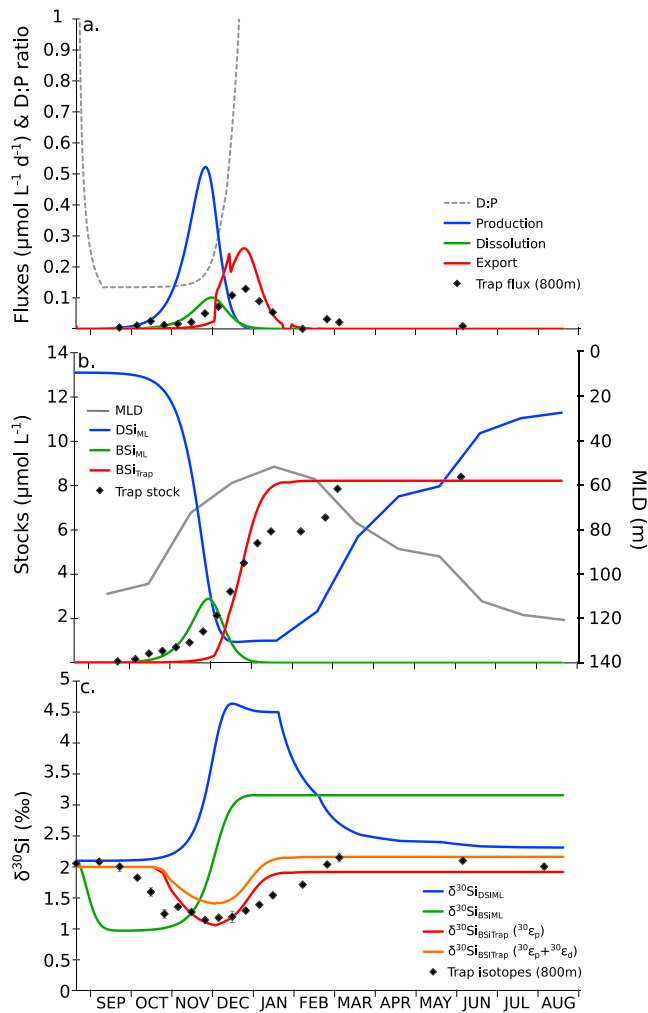


Figure 4. Model outputs simulated in the Polar Front Zone case study, compared with the flux and isotopic composition measured in the 800 m sediment trap (black diamonds; from Closset et al., 2015). (a) Simulated BSi gross production (green) and dissolution (blue) in the ML and BSi exported production at 800 m (red). (b) Simulated DSi (blue) and BSi (green) pools in the ML and BSi pool exported at 800 m (red). (c) Simulated $\delta^{30}\text{Si}$ values for DSi (blue) and BSi (green) in the ML, exported BSi with (purple) and without (red) isotopic fractionation during BSi dissolution.

et al., 2005) was not consumed by diatoms at the end of the AZ bloom, corresponding to $8.7 \mu\text{mol/L}$ remaining in the ML by early March 2002 (Figure 2a). This value is consistent with the $10 \mu\text{mol/L}$ measured in February 1999 during the SOIREE experiment in the same zone (Trull et al., 2001). Similarly, 35% of the initial DSi stock (i.e., $3.9 \mu\text{mol/L}$) remained in the PFZ ML at the end of the productive period (Figure 2c), consistent with the range of DSi concentrations observed during March–April in this zone (from 1 to $4 \mu\text{mol/L}$; e.g., Fripiat et al., 2011a; Trull et al., 2001; Bowie et al., 2011). Finally, considering the lightening of the $\delta^{30}\text{Si}_{\text{BSi}}$ signal in the AZ associated with vertical mixing in March 2002, the silicic acid flux into the ML during this event was estimated to be approximately 20% of the DSi initial pool. This $5.6 \mu\text{mol/L}$ supply is reasonable considering Brzezinski et al. (2001) and Nelson et al. (2001) have measured similar increases of DSi concentrations in the AZ surface waters between January and March 1998.

For the deeper PFZ trap, good matches were not obtained with either the open or closed models, using the $\delta^{30}\text{Si}$ and concentration of DSi measured by Cardinal et al. (2005) 2 years after the mooring implementation. The data do show the exponential increase of $\delta^{30}\text{Si}_{\text{inst}}$ that characterizes a Rayleigh fractionation law, but they do not fit any of the theoretical $\delta^{30}\text{Si}_{\text{BSi}}$ evolutions (see Figure S1). Several hypotheses can be formulated to explain this: As aforementioned, it is possible that the appropriate initial parameters were not used, confounding model constraints and providing unrealistic predictions. (ii) Moreover, it has been shown that natural systems can proceed in a mixed way between open and closed systems (Fry, 2006). These systems would display intermediate results between the two ideal situations, depending on the Si-consumption:supply ratio. In the PFZ, the proximity of the front may have produced instabilities in the ML, facilitating nutrient and material exchanges between surface and deep waters. These scenarios might lead the system to behave in a way that cannot be described by either of the two ideal and simple models. Our results show that while these models are useful from a paleoceanographic perspective to record interannual changes in the ML DSi consumption, neither of them can be used to satisfactorily interpret the seasonal and spatial variations of the $\delta^{30}\text{Si}$ of exported BSi. To better address the variability of the $\delta^{30}\text{Si}$ of settling particles, we have compared our time series with a biogeochemical model of Si mass and isotope cycling that integrates the combined effect of different processes controlling the Si cycle in the AZ and the PFZ (Figure 3).

3.2. Modern Applications of the Box Model

3.2.1. Si Biogeochemical Cycle and Diatom History in the PFZ and AZ

The model successfully produced a spring bloom of diatoms peaking at the end of November in the PFZ and in January in the AZ. This resulted in maximal concentrations of BSi in the ML of 2.9 and $8.5 \mu\text{mol/L}$ in the PFZ and AZ, respectively (Figures 4b and 5b); values that are consistent with extensive surveys south of Australia (Trull et al., 2018). In the PFZ, the maximal BSi gross production produced by the model ($0.52 \mu\text{mol L}^{-1} \text{d}^{-1}$) fits well with the range of expected spring values (e.g., $0.58 \mu\text{mol L}^{-1} \text{d}^{-1}$ in the Indian Sector, Closset et al., 2014, or from 0.17 to $0.80 \mu\text{mol L}^{-1} \text{d}^{-1}$ in the Atlantic Sector; Quéguiner & Brzezinski, 2002). Interestingly, the maximal gross-production predicted by the model in the AZ ($1.6 \mu\text{mol L}^{-1} \text{d}^{-1}$) is much higher than previous values measured in the Southern Ocean ML (e.g., from 0.24 to $0.67 \mu\text{mol L}^{-1} \text{d}^{-1}$ above the Kerguelen Plateau characterized by intense diatom bloom due to the alleviation of Fe-limitation, Closset et al., 2014, or from 0.02 to $0.35 \mu\text{mol L}^{-1} \text{d}^{-1}$ in the Pacific Sector, Brzezinski et al., 2001). These discrepancies may reflect overestimates of dissolution during particle settling by the

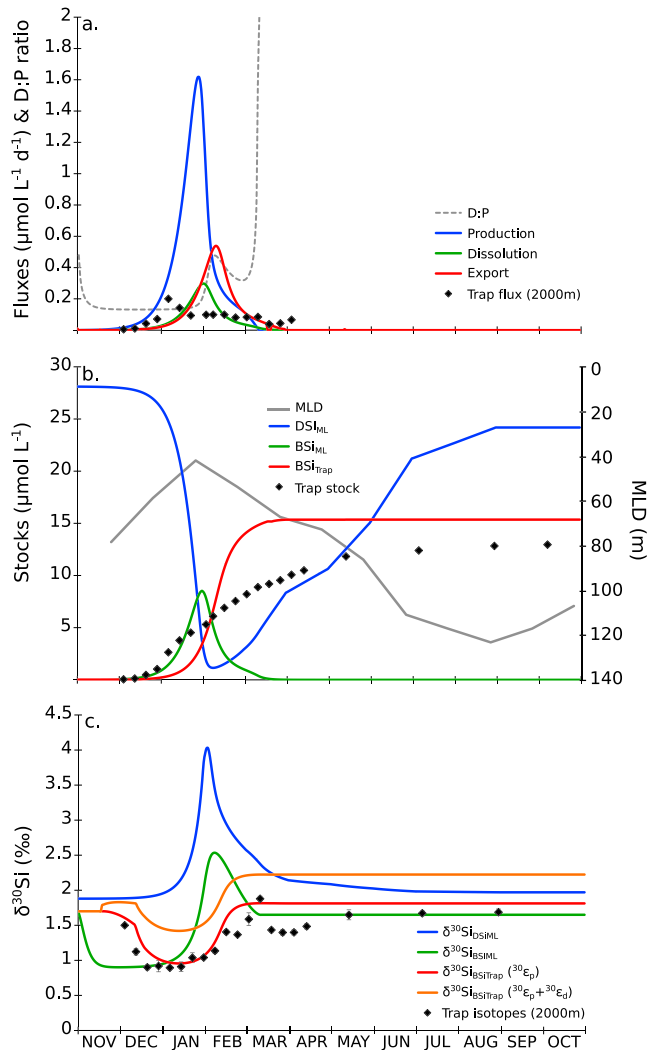


Figure 5. Model outputs simulated in the Antarctic Zone case study, compared with the flux and isotopic composition measured in the 2,000-m sediment trap (black diamonds; from Closset et al., 2015). (a) Simulated BSi gross-production (green) and dissolution (blue) in the ML, and BSi exported production at 2,000 m (red). (b) Simulated DSi (blue) and BSi (green) pools in the ML and BSi pool exported at 2,000 m (red). (c) Simulated $\delta^{30}\text{Si}$ values for DSi (blue) and BSi (green) in the ML, exported BSi with (purple) and without (red) isotopic fractionation during BSi dissolution.

model and/or the scarcity of in situ measurements (especially at the peak of the bloom) which may miss the actual maximal value of this parameter. Consequently, these modelled blooms have artificially depleted the silicic acid stock in the ML with DSi concentrations decreasing to 0.77 and 1.15 $\mu\text{mol/L}$ in December in the PFZ and in February in the AZ, respectively. Then, dissolution in the ML and export to the deep ocean reduced the stock of BSi and prevented particle accumulation in the ML. Instead BSi accumulated in the sediment traps, where it reached an integrated stock of 619 and 1,362 mmol/m^2 in the PFZ and AZ, respectively, which is in good agreement with our observations (638 and 1,257 mmol/m^2 in the PFZ and AZ, respectively). The estimated export flux peaked approximately 1 month after the bloom maxima in the ML, in agreement with previous studies, reflecting the delay due to settling processes (Closset et al., 2015; Rigual-Hernández et al., 2015; 2016). Note that even when the final mass balance is maintained in the model, the magnitude and the extent of the export fluxes were different from the observations in both zones. For example, the peak flux of particles in the PFZ calculated from the trap data was approximately 3 times lower than that predicted by the model, but it is more widely distributed during the season (Figure 4a). This suggests that at least one process tempering the export of diatoms is missing or misestimated in the model. For instance, differentiating the living and detrital BSi pools, with the first being involved only in the production process and the latter only in the dissolution process, might help to refine our representation of the Si cycling in the ML were unknown. However, since mortality rate of phytoplankton in the ML is unknown, a component representing detrital diatom frustules was not included in the model.

3.2.2. $\delta^{30}\text{Si}$ Seasonal Evolution in the ACC ML and Export to Depth

Simulated $\delta^{30}\text{Si}$ signatures of exported BSi match relatively well with those actually observed in the traps (800 m in the PFZ and 2,000 in the AZ, Figures 4c and 5c, respectively), indicating that the box model adequately describes the main drivers of seasonal variations in $\delta^{30}\text{Si}$ of sinking particles in the Southern Ocean (see section 3.2.3). This approach allows us to discuss the seasonal variations of $\delta^{30}\text{Si}$ in the other Si pools (e.g., in the ML).

During the productive period (from mid-September to the end of January in the PFZ and from early December to the end of February in the AZ), the $\delta^{30}\text{Si}$ of BSi was 1.13‰ or 0.98‰ lower than the $\delta^{30}\text{Si}$ of DSi in the ML due to the isotopic fractionation during uptake (De La Rocha et al., 1997). The apparent fractionation factor ($\Delta^{30}\text{Si} = \delta^{30}\text{Si}_{\text{DSi}} - \delta^{30}\text{Si}_{\text{BSi}}$) stayed constant

during the high Si uptake: Si supply and low D:P ratio period but changed later in the season. This is confirmed by sediment trap observations indicating that exported BSi is close to the Rayleigh instantaneous product for which a constant isotopic offset (i.e., $^{30}\epsilon$) with silicic acid is expected. Once the DSi concentration became limiting to Si uptake, the Si uptake: Si supply ratio decreased and the supply of isotopically lighter Si via vertical mixing decreased the $\delta^{30}\text{Si}$ of the ML DSi pool. The $\delta^{30}\text{Si}_{\text{BSi}}$ was affected differently. In the PFZ, BSi is accumulated in the ML only when the water column experienced strong stratification, preventing the supply of new DSi from the WW. Since BSi did not accumulate later in the season in the ML, the BSi isotopic signature remained high during winter, lowering $\Delta^{30}\text{Si}$ and allowing the very low amount of remaining BSi in the ML to become (if measured at this time of the year) heavier than the DSi pool (Figure 4c). This observation illustrates, in accordance with previous studies, that the combination of simple processes such as accumulation versus export of BSi and/or uptake versus supply of DSi in the ML are sufficient to explain the low $\Delta^{30}\text{Si}$ observed by Fripiat et al. (2012) and Closset et al. (2016) in the PFZ and above the Kerguelen Plateau when the ML DSi pool was highly depleted at the end of summer. Similar dynamics

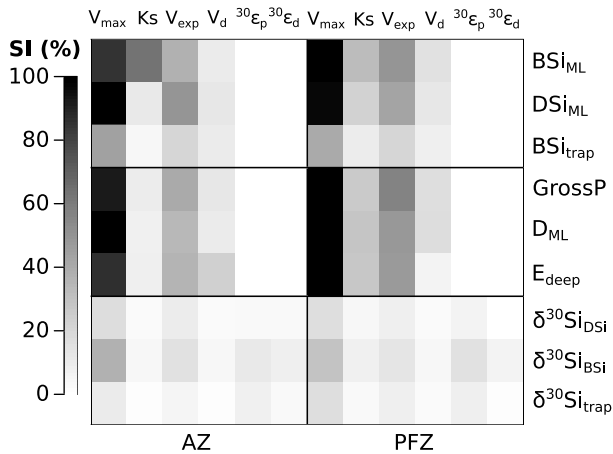


Figure 6. Sensitivity indices of simulated concentrations and isotopic signatures in the different model boxes. Colors express the response range of the fluxes, concentrations, and deltas, with high sensitivity in dark color and low sensitivity in white color. ML = mixed layer.

occurred in the AZ. There, strong vertical mixing events that deepened the ML at the end of the productive period brought new and isotopically light DSi from the WW to the ML, allowing diatoms to produce frustules with lower $\delta^{30}\text{Si}$ (Closset et al., 2015). Since this ML disruption occurs when the BSi net production in the ML is still significant, the isotopic signature of BSi that accumulates in the ML decreases by 0.9 ‰ (Figure 5c). This behavior is also recorded 1 month later in our sediment traps which corresponds exactly to the delay estimated between the production in the ML and the export of particles at depth (Closset et al., 2015).

3.2.3. Sensitivity Analysis

An important objective of the current study is to use the model to identify the dominant processes acting on the seasonal variations of BSi production and Si cycling in the ML and at depth using exported BSi $\delta^{30}\text{Si}$ signatures. Note that since the box model outcomes are associated with high uncertainties, simulations should not be used to make quantitative interpretations. It is however interesting to investigate the sensitivity of the presented results to the main selections made for the model setup. To identify the major contributing parameter to the model outcomes, the box model has been run several times, each time varying parameters listed

in Table 1 from -5% to $+5\%$ (using 0.5% steps) around their calibration (default) values. The effect of these variations on each model output can be estimated by calculating a sensitivity index (SI) as follows:

$$SI = \sqrt{\frac{1}{N} \sum_{t=1}^N \left(\frac{|y_{\max(t)} - y_{\min(t)}|}{y_{\text{cal}(t)}} \right)^2} \quad (22)$$

where y_{\max} , y_{\min} , and y_{cal} are the model outputs obtained with parameter set to its $+5\%$, -5% , and default values, respectively. This method, proposed in De Brauwere et al. (2012), allows one to compare relative change in parameters with relative change in model outputs.

The most important parameter that controls the behavior of the model is V_{\max} , the maximal rate of Si uptake that diatoms can achieve when they are saturated with DSi (see Figure 6). For example, varying V_{\max} by 5% causes a variation of more than 100% in terms DSi concentration in the ML at a given time and of more 40% of the BSi reaching the traps in both the AZ and PFZ. It changes the Si fluxes between the different compartments by a factor of more than 100% in the PFZ and up to 232% for the dissolution in the AZ ML, with most of these effects being confined to the production period. While it is still the most important parameter, it only mildly affects the Si isotopes (e.g., $\delta^{30}\text{Si}$ of diatoms collected in the traps vary by 11%, and 17% in the AZ and PFZ, respectively). Changes to V_{\max} on the $\delta^{30}\text{Si}$ values alters both the magnitude and the timing of the peak (e.g., increasing trend in the traps delayed by approximately three weeks between the -5% and the $+5\%$ run in both zones).

Most variables mildly react to variations in V_{exp} , the parameter linking the standing stock to the export flux of BSi from the ML. This parameter is the second most sensitive parameter in the model with the largest influence again observed during the productive period (e.g., accumulation of BSi, BSi flux and $\delta^{30}\text{Si}$ in the traps change by 21%, 37%, and 6%, respectively, in the AZ and by 21%, 48%, and 9%, respectively, in the PFZ). The half saturation constant (Ks) is an inverse measure of the diatom silicic acid affinity. Therefore, decreasing Ks allowed diatoms to take up DSi more rapidly at lower DSi concentrations. Changing Ks had a limited effect in the AZ with less than 12% (except for BSi concentration in the ML) and an intermediate effect in the PFZ with 30% variability in terms of Si stocks and fluxes and less than 10% variability for Si isotopes. Finally, altering the dissolution rates had virtually no impact on silicon isotopes ($<5\%$) and very low impact on Si stocks and fluxes in the model ($<24\%$) for both zones. This parameter contributes more at the end of the productive period and during winter when it controls the accumulation of BSi in the traps.

As expected, the fractionation factors (α_{prod} and α_{diss}) only influence the delta values (Figure 6). However, the sensitivity of the model to these factors is relatively low with the largest variations on $\delta^{30}\text{Si}_{\text{BSi}}$ in the

ML for both case (12% and 16% changes in the AZ and PFZ, respectively), implying that the results obtained will still be robust if the isotopic fractionation factors deviate slightly from their calibration values.

3.3. Paleoapplications of the Model

The time-integrated $\delta^{30}\text{Si}$ of exported BSi collected by our sediment traps or simulated by the model (1.59‰ and 1.29‰ in the PFZ and AZ, respectively) reflects the extent of DSi consumption at the time when net BSi production and diatom accumulation are maximal in the ML (Figures 4b and 5b). Most of the time, this corresponds to the minima in annual silicic acid concentration (e.g., in the AZ) but not always. For example, this occurs in the PFZ, with a consumption of 54% of the initial stock corresponding to a DSi pool of 6.05 $\mu\text{mol/L}$ instead of the 0.77 $\mu\text{mol/L}$ remaining at the end of the productive period. It allows us to temper the hypothesis of Egan et al. (2012) suggesting that since diatom $\delta^{30}\text{Si}$ data set from core tops displays a better correlation with surface water minimum annual DSi concentrations, the $\delta^{30}\text{Si}$ proxy documents the seasonal maximum of diatom silicic acid utilization instead of the mean annual DSi utilization. In our study, the isotopic signal stored in settling particles records the DSi drawdown during the peak of the diatom bloom (i.e., at the biomass maximum and not the conditions at the end of summer). This has important implications for the interpretation of paleoceanographic archives. Indeed, since this period of the year displays a very low D:P and Si supply: Si-uptake ratios, the relationship between the relative consumption of silicic acid and the isotopic signature of diatoms in the ML is preserved. We can then assume that from a paleoceanographic perspective, the system behaves like a closed model and can be simply described using Rayleigh equations as suggested in Fripiat et al. (2012).

Previous studies have suggested that the effects of fractionation during dissolution should be considered when interpreting paleoceanographic reconstructions based on $\delta^{30}\text{Si}$ (e.g., Coffineau et al., 2014). This simple model, combined with the sediment trap time series, gives the opportunity to test the effect of silicon isotope fractionation during dissolution of BSi in the water column. By adding a fractionation factor of -0.55‰ (Demarest et al., 2009) during the dissolution of BSi in the ML and during the particle settling in the deep-water, the $\delta^{30}\text{Si}_{\text{DSi}}$ and $\delta^{30}\text{Si}_{\text{BSi}}$ become, respectively, lighter and heavier both in the PFZ and AZ, in agreement with a decrease in the net fractionation factor (see Fripiat et al., 2012). The $\delta^{30}\text{Si}$ of exported BSi became $0.22\text{‰} \pm 0.1\text{‰}$ heavier in the PFZ and $0.42\text{‰} \pm 0.13\text{‰}$ heavier in the AZ, no longer fitting the $\delta^{30}\text{Si}$ values measured in the sediment trap (Figures 4c and 5c). This effect is especially pronounced in the AZ where a greater proportion of the BSi produced in the ML might be dissolved before reaching the sediment trap (due to its deeper location). Combined with previous observations from the sediment trap time-series (see Closset et al., 2015), these simulations agree with the absence of an isotopic effect during the dissolution of BSi in the water column.

4. Conclusions

The main objective of our study was to investigate the variability in the magnitude, timing and isotopic composition of siliceous particles from the surface to the deep ocean using a combination of a modelling approach and seasonal records of $\delta^{30}\text{Si}$ of exported BSi in the AZ and PFZ. The box model presented here describes the time evolution, both for concentration and isotopic composition, of DSi and BSi in the ML and at depth. It integrates the seasonal variations of processes affecting the Si biogeochemical cycle such as uptake, dissolution, settling and mixing. It differs considerably from the previous models by integrating processes that affect the fate of particles and the magnitude of BSi recycling through the water column. In addition, and for the first time, it uses information from in situ measurements (fluxes and isotopic composition) recorded during the whole year which helps to better constrain the model outcomes and provides robust information about the seasonal variations of $\delta^{30}\text{Si}$ of exported BSi in the Southern Ocean.

From a modern perspective, the simulated $\delta^{30}\text{Si}$ signatures of exported BSi match relatively well with those actually measured in situ, indicating that we have adequately described the main drivers of the seasonal variations in the $\delta^{30}\text{Si}$ of sinking particles in the Southern Ocean. The model allows us to quantify fluxes of Si in and out the ML associated to export and/or mixing, illustrating that the combination of simple processes such as accumulation vs. export of BSi and/or uptake versus supply of DSi in the ML are sufficient to explain the seasonal variations of $\Delta^{30}\text{Si}$ previously observed in the literature. It also suggests that the maximal rate of

Si uptake (V_{\max}) in the ML, more than other processes such as dissolution or export, is the most important process in the controls of $\delta^{30}\text{Si}$ signatures of both BSi and DSI.

From a paleoceanographic perspective, the system behaves very similarly to a closed model and can be simply described using Rayleigh equations. However, the time-integrated $\delta^{30}\text{Si}$ of exported BSi measured in the sediments reflects the extent of DSI consumption at the time when net BSi production and diatom accumulation are maximum in the ML contrary to reports from previous studies. Using that assumption, the fractionation factor calculated in the AZ is slightly but not significantly different from the fractionation factor in the PFZ ($-0.98\text{‰} \pm 0.13\text{‰}$ and $-1.13\text{‰} \pm 0.16\text{‰}$, respectively). Finally, our simulations support the absence of an isotopic effect during the dissolution of BSi in the water column and confirm that the $\delta^{30}\text{Si}$ of diatom is a reliable proxy for silicic acid utilization in the past ocean.

Acknowledgments

The research leading to these results has received funding from the European Union Seventh Framework Program under the grant agreement 294146 (MuSiCC Marie Curie CIG) and contributes to the GEOTRACES program. The SAZ sediment trap program received support from the Australian Integrated Marine Observing System, Australian Antarctic Climate and Ecosystems Cooperative Research Center, Australian Antarctic Sciences awards 1156 and 2256, the Australian Marine National Facility, the U.S. NSF Office of Polar Programs, and the Belgian Science and Policy Organization. The authors are especially grateful to Mark Brzezinski and Heather McNair for their constructive and helpful discussions about the model and Nicholas Baetge for correction of English. The authors also thank G. De Souza, one anonymous reviewer, and the associate editor for their constructive comments that helped us improving the manuscript. Data used in this study are available in the supporting information of the previous companion paper Closset et al. (2015).

References

- Bidle, K. D., & Azam, F. (1999). Accelerated dissolution of diatom silica by marine bacterial assemblages. *Nature*, 397(6719), 508–512. <https://doi.org/10.1038/17351>
- Bowie, A. R., Griffiths, F. B., Dehairs, F., & Trull, T. W. (2011). Oceanography of the Subantarctic and Polar Frontal Zones south of Australia during summer: Setting for the SAZ-Sense study. *Deep Sea Research, Part II*, 58(21–22), 2059–2070. <https://doi.org/10.1016/j.dsr2.2011.05.033>
- Brzezinski, M. A., Nelson, D. M., Franck, V. M., & Sigmon, D. E. (2001). Silicon dynamics within an intense open-ocean diatom bloom in the Pacific sector of the Southern Ocean. *Deep Sea Research, Part II*, 48(19–20), 3997–4018. [https://doi.org/10.1016/S0967-0645\(01\)00078-9](https://doi.org/10.1016/S0967-0645(01)00078-9)
- Brzezinski, M. A., Pride, C. J., & Frank, V. M. (2002). A switch from $\text{Si}(\text{OH})_4$ to NO_3^- depletion in the glacial Southern Ocean. *Geophysical Research Letters*, 29(12), 1564. <https://doi.org/10.1029/2001GL014349>
- Cardinal, D., Alleman, L. Y., Dehairs, F., Savoye, N., Trull, T. W., & André, L. (2005). Relevance of silicon isotopes to Si-nutrient utilization and Si-source assessment in Antarctic waters. *Global Biogeochemical Cycles*, 19, GB2007. <https://doi.org/10.1029/2004GB002364>
- Cavagna, A. J., Fripiat, F., Dehairs, F., Wolf-Gladrow, D., Cisewski, B., Savoye, N., et al. (2011). Silicon uptake and supply during a Southern Ocean iron fertilization experiment (EIFEX) tracked by Si isotopes. *Limnology and Oceanography*, 56(1), 147–160. <https://doi.org/10.4319/lo.2011.56.1.0147>
- Closset, I., Cardinal, D., Bray, S. G., Thil, F., Djouaev, I., Rigual-Hernandez, A. S., & Trull, T. W. (2015). Seasonal variations, origin, and fate of settling diatoms in the Southern Ocean tracked by silicon isotope records in deep sediment traps. *Global Biogeochemical Cycles*, 29, 1495–1510. <https://doi.org/10.1002/2015GB005180>
- Closset, I., Cardinal, D., Rembauville, M., Thil, F., & Blain, S. (2016). Unveiling the Si cycle using isotopes in an iron-fertilized zone of the Southern Ocean: From mixed-layer supply to export. *Biogeosciences*, 13(21), 6049–6066. <https://doi.org/10.5194/bg-13-6049-2016>
- Closset, I., Lasbleiz, M., Leblanc, K., Quéguiner, B., Cavagna, A. J., Elskens, M., et al. (2014). Seasonal evolution of net and regenerated silica production around a natural Fe-fertilized area in the Southern Ocean estimated with Si isotopic approaches. *Biogeosciences*, 11, 5827–5846. <https://doi.org/10.5194/bg-11-5827-2014>
- Coffineau, N., De La Rocha, C. L., & Pondaven, P. (2014). Exploring interacting influences on the silicon isotopic composition of the surface ocean: A case study from the Kerguelen Plateau. *Biogeosciences*, 11(5), 1371–1391. <https://doi.org/10.5194/bg-11-1371-2014>
- De Brauwere, A., Fripiat, F., Cardinal, D., Cavagna, A. J., De Ridder, F., André, L., & Elskens, M. (2012). Isotopic model of oceanic silicon cycling: The Kerguelen Plateau case study. *Deep Sea Research, Part I*, 70, 42–59. <https://doi.org/10.1016/j.dsr.2012.08.004>
- De La Rocha, C. L., Brzezinski, M. A., & DeNiro, M. J. (1997). Fractionation of silicon isotopes by marine diatoms during biogenic silica formation. *Geochimica et Cosmochimica Acta*, 61(23), 5051–5056. [https://doi.org/10.1016/S0016-7037\(97\)00300-1](https://doi.org/10.1016/S0016-7037(97)00300-1)
- De La Rocha, C. L., Brzezinski, M. A., DeNiro, M. J., & Shemesh, A. (1998). Silicon-isotope composition of diatoms as an indicator of past oceanic change. *Nature*, 395(6703), 680–683. <https://doi.org/10.1038/27174>
- De Souza, G. F., Slater, R. D., Dunne, J. P., & Sarmiento, J. L. (2014). Deconvoluting the controls on the deep ocean's silicon stable isotope distribution. *Earth and Planetary Science Letters*, 398, 66–76. <https://doi.org/10.1016/j.epsl.2014.04.040>
- Demarest, M. S., Brzezinski, M. A., & Beucher, C. P. (2009). Fractionation of silicon isotopes during biogenic silica dissolution. *Geochimica et Cosmochimica Acta*, 73(19), 5572–5583. <https://doi.org/10.1016/j.gca.2009.06.019>
- DeMaster, D. (1981). The supply and accumulation of silica in the marine environment. *Geochimica et Cosmochimica Acta*, 45(10), 1715–1732. [https://doi.org/10.1016/0016-7037\(81\)90006-5](https://doi.org/10.1016/0016-7037(81)90006-5)
- Egan, K. E., Rickaby, R. E. M., Leng, M. J., Hendry, K. R., Hermoso, M., Sloane, H. J., et al. (2012). Diatom silicon isotopes as a proxy for silicic acid utilisation: A Southern Ocean core top calibration. *Geochimica et Cosmochimica Acta*, 96, 174–192. <https://doi.org/10.1016/j.gca.2012.08.002>
- Eppley, R. W. (1972). Temperature and phytoplankton growth in the sea. *Fishery Bulletin*, 70(4), 1063–1085.
- Franck, V. M., Bruland, K. W., Hutchins, D. A., & Brzezinski, M. A. (2003). Iron and zinc effects on silicic acid and nitrate uptake kinetics in three high-nutrient, low chlorophyll (HNLC) regions. *Marine Ecology Progress Series*, 252, 15–33. <https://doi.org/10.3354/meps252015>
- Fripiat, F., Cavagna, A.-J., Dehairs, F., de Brauwere, A., André, L., & Cardinal, D. (2012). Processes controlling the Si-isotopic composition in the Southern Ocean and application for paleoceanography. *Biogeosciences*, 9(7), 2443–2457. <https://doi.org/10.5194/bg-9-2443-2012>
- Fripiat, F., Cavagna, A. J., Dehairs, F., Speich, S., André, L., & Cardinal, D. (2011a). Silicon pool dynamics and biogenic silica export in the Southern Ocean inferred from Si-isotopes. *Ocean Science*, 7(5), 533–547. <https://doi.org/10.5194/os-7-533-2011>
- Fripiat, F., Cavagna, A. J., Savoye, N., Dehairs, F., André, L., & Cardinal, D. (2011b). Isotopic constraints on the Si-biogeochemical cycle of the Antarctic Zone in the Kerguelen area (KEOPS). *Marine Chemistry*, 123(1–4), 11–22. <https://doi.org/10.1016/j.marchem.2010.08.005>
- Fry, B. (2006). *Stable isotope ecology*. New York: Springer Science Business Media LLC. <https://doi.org/10.1007/0-387-33745-8>
- Holzer, M., Primeau, F. W., DeVries, T., & Matear, R. (2014). The Southern Ocean silicon trap: Data-constrained estimates of regenerated silicic acid, trapping efficiencies, and global transport paths. *Journal of Geophysical Research: Oceans*, 119, 313–331. <https://doi.org/10.1002/2013JC009356>

- Kamatani, A. (1982). Dissolution rates of silica from diatoms decomposing at various temperatures. *Marine Biology*, 68(1), 91–96. <https://doi.org/10.1007/BF00393146>
- Nelson, D. M., Brzezinski, M. A., Sigmon, D. E., & Franck, V. M. (2001). A seasonal progression of Si limitation in the Pacific sector of the Southern Ocean. *Deep Sea Research, Part II*, 48(19–20), 3973–3995. [https://doi.org/10.1016/S0967-0645\(01\)00076-5](https://doi.org/10.1016/S0967-0645(01)00076-5)
- Paasche, E. (1973). Silicon and the ecology of marine plankton diatoms. II. Silicate-uptake kinetics in five diatom species. *Marine Biology*, 19(3), 262–269. <https://doi.org/10.1007/BF02097147>
- Panizzo, V., Crespin, J., Crosta, X., Shemesh, A., Massé, G., Yam, R., et al. (2014). Sea ice diatom contributions to Holocene nutrient utilization in East Antarctica. *Paleoceanography*, 29, 328–343. <https://doi.org/10.1002/2014PA002609>
- Pondaven, P., Ragueneau, O., Tréguer, P., Hauvespre, A., dezileau, L., & Reyss, J. L. (2000). Resolving the ‘opal paradox’ in the Southern Ocean. *Nature*, 405(6783), 168–172. <https://doi.org/10.1038/35012046>
- Quéguiner, B., & Brzezinski, M. A. (2002). Biogenic silica production rates and particulate organic matter distribution in the Atlantic sector of the Southern Ocean during austral spring 1992. *Deep Sea Research, Part II*, 49(9–10), 1765–1786. [https://doi.org/10.1016/S0967-0645\(02\)00011-5](https://doi.org/10.1016/S0967-0645(02)00011-5)
- Ragueneau, O., Tréguer, P., Leynaert, A., Anderson, R. F., Brzezinski, M. A., DeMaster, D. J., et al. (2000). A review of the Si cycle in the modern ocean: Recent progress and missing gaps in the application of biogenic opal as a paleoproductivity proxy. *Global and Planetary Change*, 26(4), 317–365. [https://doi.org/10.1016/S0921-8181\(00\)00052-7](https://doi.org/10.1016/S0921-8181(00)00052-7)
- Reynolds, B. C., Aggarwal, J., André, L., Baxter, D., Beucher, C., Brzezinski, M. A., et al. (2007). An inter-laboratory comparison of Si isotope reference materials. *Journal of Analytical Atomic Spectrometry*, 22(5), 561–568. <https://doi.org/10.1039/b616755a>
- Rigual-Hernández, A. S., Trull, T. W., Bray, S. G., & Armand, L. K. (2016). The fate of diatom valves in the Subantarctic and Polar Frontal Zones of the Southern Ocean: Sediment trap versus surface sediment assemblages. *Palaeogeography, Palaeoclimatology, Palaeoecology*, 457, 129–143. <https://doi.org/10.1016/j.paleo.2016.06.004>
- Rigual-Hernández, A. S., Trull, T. W., Bray, S. G., Closset, I., & Armand, L. K. (2015). Seasonal dynamics in diatom export fluxes to the deep sea in the Australian sector of the Antarctic Zone. *Journal of Marine Systems*, 142, 62–74. <https://doi.org/10.1016/j.jmarsys.2014.10.002>
- Sallée, J. B., Wienders, N., Morrow, R., & Speer, K. (2006). Formation of Subantarctic mode water in the Southeastern Indian Ocean. *Ocean Dynamics*, 56(5–6), 525–542. <https://doi.org/10.1007/s10236-005-0054-x>
- Sarmiento, J. L., Gurber, N., Brzezinski, M. A., & Dunne, J. P. (2004). High-latitude controls of thermocline nutrients and low latitude biological productivity. *Nature*, 427(6969), 56–60. <https://doi.org/10.1038/nature02127>
- Sutton, J. N., Varela, D. E., Brzezinski, M. A., & Beucher, C. P. (2013). Species-dependent silicon isotope fractionation by marine diatoms. *Geochimica et Cosmochimica Acta*, 104, 300–309. <https://doi.org/10.1016/j.gca.2012.10.057>
- Tréguer, P. J. (2014). The Southern Ocean silica cycle. *Comptes Rendus Geoscience*, 346(11–12), 279–286. <https://doi.org/10.1016/j.crte.2014.07.003>
- Tréguer, P. J., & De La Rocha, C. L. (2013). The world ocean silica cycle. *Annual Review of Marine Science*, 5(1), 477–501. <https://doi.org/10.1146/annurev-marine-121211-172346>
- Trull, T., Passmore, A., Davies, D. M., Smit, T., Berry, K., & Tilbrook, B. (2018). Distribution of planktonic biogenic carbonate organisms in the Southern Ocean south of Australia: A baseline for ocean acidification impact assessment. *Biogeosciences*, 15(1), 31–49. <https://doi.org/10.5194/bg-15-31-2018>
- Trull, T., Rintoul, S. R., Hadfield, M., & Abraham, E. R. (2001). Circulation and seasonal evolution of polar waters south of Australia: Implications for iron fertilization of the Southern Ocean. *Deep Sea Research, Part II*, 48(11–12), 2439–2466. [https://doi.org/10.1016/S0967-0645\(01\)00003-0](https://doi.org/10.1016/S0967-0645(01)00003-0)
- Varela, D. E., Pride, C. J., & Brzezinski, M. A. (2004). Biological fractionation of silicon isotopes in Southern Ocean surface waters. *Global Biogeochemical Cycles*, 18, GB1047. <https://doi.org/10.1029/2003GB002140>
- Wetzel, F., de Souza, G. F., & Reynolds, B. C. (2014). What controls silicon fractionation during dissolution of diatom opal? *Geochimica et Cosmochimica Acta*, 131, 128–137. <https://doi.org/10.1016/j.gca.2014.01.028>